Hence, 10 stacked rock disks are used in this study to generate the long-wavelength propagation in a regularly jointed rock mass.

2.2 Sample preparation

To penetrate fine cracks and fissures, highly penetrable grouts are often employed for rock grouting. This results in a high W/C ratio, often within the range of 1 to 10. This high water content results in a very unstable grout mix, severe bleeding and long gel-time (Warner, 2004). Currently, microcement grouts are considered more effective for rock grouting compared to OPC grouts as it has a much smaller particle size and thus, results in greater grout strength, better penetration and less bleeding. Setting agents are often added to control the gel-time of grouts for field applications. In the past, silicate-based agents such as water glass were widely applied to control setting times of cementitious grouts. However, silicate grouts lose cohesion and degrade easily in areas of high ground water flow, resulting in poor durability and ground water pollution and making it unsuitable for permanent ground improvement (Delfosse-Ribay et al., 2004). Currently, the use of silicate-based setting agents have been prohibited in Europe and Japan (Gouvenot, 1987). An environmentally friendly alternative is calcium aluminates, which occur naturally in Portland cement in the form of C_2A. Calcium aluminates such as $C_{12}A_7$, $C_{11}A_7$, CaA_2 or C_4A_3S react with water and $Ca(OH)_2$ and $CaSO_4$ in cement to form a needle-shaped crystalline matrix that contributes to high early strength gain (Park et al., 2008). For the aforementioned calcium aluminate forms, $C_{12}A_7$ has the fastest hydration reaction and displays hardening within 1 to 3 minutes after water contact.

The grout used in this study is a cement milk composed of microcement and water with a water-to-cement ratio of 100%. Amorphous $C_{12}A_7$ corresponding to 5% the mass of microcement was added as a setting agent and thoroughly mixed with the microcement before the addition of water to achieve an even distribution. The grout specimens are made using a PVC mold and PVC pipe running along the center to create a hollow cylindrical specimen. The rock used in this study is Machun granite commonly found in Korea. Smooth surfaced rock disks are created by cutting rock columns using a diamond saw and smoothing the surfaces with sand paper. Central holes are made at the center of each disk using a water jet. Grouting of rock joints was simulated by pasting contiguous rock disks for 2mm thickness with the microcement grout. The properties of the rocks used in this study are shown in Table 1.

Table. 1 Properties of Machun granite used in this study

Configuration	Machun stone	Grout
Joint condition	Planar	**-**
Average joint thickness (mm)	2.0	-
Outer diameter(mm)	63.0	62.4

Inner diameter(mm)	24.0	25.0
Length(mm)	268.5	295.0
Density (kg/m^3)	2797	1859
Number of discs in column	10	-

2.3 Experimental setup

The rock mass dynamic test device developed by Kim (2008) is a modified Stokoe-type resonant column test device that can successfully determine the strain-dependent properties of an equivalent continuum rock column in the mid-strain range (10^{-5} to 10^{-3}). A schematic diagram of the apparatus is shown in Figure 1. The jointed rock specimen is secured at the bottom to the high impedance steel base to create a fixed-free boundary condition. Axial loading is applied using thin rod that anchors the light steel cap secured at the top of the specimen to the steel base. The bottom end of the rod is attached to a lever system that can apply axial loads up to 2 MPa. The driving system is modified to produce large torsional excitations sufficient for testing rock masses. Current is supplied to the coil-magnet system using a current amplifier (Eliezer EA160AR) to create torsional excitation in the drive plate. The torsional movement is measured using a pair of accelerometers (PCB 353B51) attached at opposing ends of the drive plates located at 106mm from the axis of rotation. The accelerometer signals are converted using a signal conditioner (PCB 482A16) and added to each other to remove the flexural mode signals. The signals are monitored using a DAQ board (PXI-6071E) and an analog channel (BNC-2120) and analyzed using a LabView program.

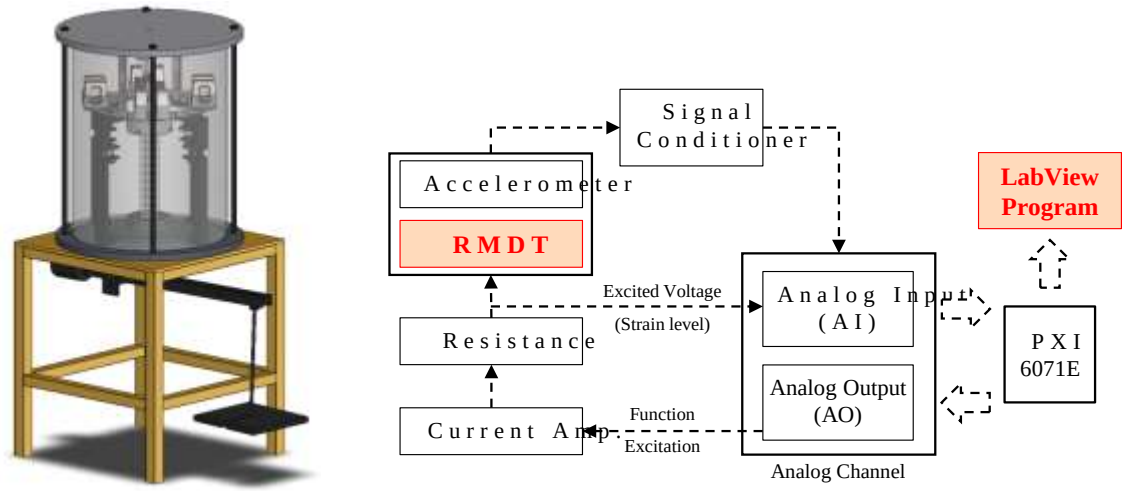

Fig. 1 Schematic diagram of RMDT device (Chong et al., 2014)

The dynamic response of the specimen is measured using the accelerometers. A frequency sweep is conducted to find the resonant frequency of the specimen. The resonant frequency is subsequently used to calculate the shear wave velocity V_S using the following equation.

$$\frac{I+I_c}{I_c}=\frac{2\pi f_r l}{V_S}\times\tan\left(\frac{2\pi f_r l}{V_S}\right) \tag{2}$$

where I is the mass polar moment of inertia of the specimen, I_c is the mass polar moment of inertia of the central rod, I_d is the mass polar moment of inertia of the drive system secured on to the specimen, l is the length of the specimen, and f_r is the resonant frequency of the specimen obtained from the frequency response curve. The shear modulus (G) was then calculated from shear wave velocity using the following equation.

$$G = \rho \times V_S^2 \tag{3}$$

where ρ is the mass density of the specimen. The material damping ratio (D) was calculated from the frequency response curve using the half power bandwidth method as follows (Richart et al., 1970):

$$D = \frac{f_{right} - f_{left}}{2 f_r} \times 100\% \tag{4}$$

where f_1 and f_2 are the half power frequencies corresponding to $V_{max}/\sqrt{2}$ where V_{max} is the peak output voltage of the frequency response curve.

2.4 Experimental procedure

The intact grout and grouted rock specimens used in this study are shown in Figure 2. Resonant column tests were conducted on the jointed rock specimen at 1000 kPa axial stress before grouting using the RMDT device. The grout specimen and grouted rock specimens were created and cured in water for 7 days before testing. The strain-dependent shear modulus and damping ratio of the test specimens at the mid strain range (10^{-5}-10^{-3}) for 1000 kPa axial stress were measured. The results before and after grouting were analysed to determine the effects of grouting and degree of improvement.

Fig. 2 Grout and grouted rock specimen used in this study

3. RESULTS AND ANALYSIS

The strain-dependent shear modulus and damping ratio of the grout, jointed rock and grouted rock specimens are shown in Figure 3. All specimens display a nonlinear

decrease in shear modulus and increase in damping ratio with increasing shear strain. The grout specimen displays a maximum shear modulus of 1.78 GPa at low strain levels, which is smaller than the values for both the ungrouted and grouted rock specimens. The maximum shear modulus of jointed rock is 2.56 GPa and with grouting, the value increases by 262% to 6.70 GPa. For all strain levels, the grouted rock specimen displays a larger shear modulus than the jointed rock specimen. This shear modulus increase is due to the improved joint stiffness with grouting. Grouting has both a cementation and joint filling effect that improves the adhesion between adjacent rock disks. Similar phenomena is also shown for the damping ratio. The minimum damping ratio of the jointed rock specimen is 5.14% and is considerably larger than the values for the grout and grouted rock specimen, which are 2.84% and 2.86% respectively. The adhesion between rock disks due to grouting reduces the attenuation of waves at the joint-joint interface. Hence, elastic wave propagation is improved and the grouted rock specimen behaves as an anisotropic intact rock.

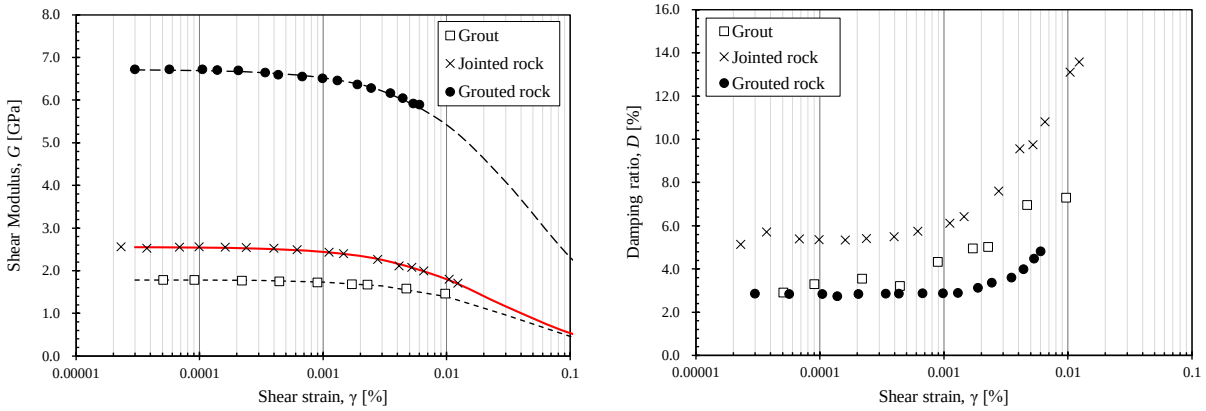

(a) Shear modulus (b) Damping ratio

Fig. 3 Strain-dependent properties of grout, jointed rock and grouted rock specimens

The normalized shear modulus degradation curves and normalized damping ratio data are shown in Figure 4. The shear modulus degradation curve was modelled using the modified hyperbolic model suggested by Darendeli (1997):

$$\frac{G}{G_{\max}} = \frac{1}{1+\left(\frac{\gamma}{\gamma_{ref}}\right)^{\alpha}} \tag{5}$$

Here, α is the coefficient of curvature which determines the degree of curvature of the normalized modulus degradation curve. The reference strain γ_{ref} corresponds to the strain amplitude when shear modulus is at $0.5G_{max}$. However, the strain range tested in this study was insufficient to cause such large γ_{ref} values. Hence, the normalized modulus degradation curve was interpolated to best fit the experimental data.

The normalized shear modulus degradation curves in Figure 4(a) display a dramatic change in the strain-dependent characteristics of jointed rocks with grouting. Ungrouted rocks display a shorter shear modulus compared to the grout specimen. With grouting, the γ_{ref} of the rock specimen increases as the grouted joints provide shear resistance and increases its linear range. The grout and grouted rock specimen display similar modulus degradation tendencies, which indicates that the grouted joints governs the shearing behaviour of grouted rocks to some degree. In comparison, the change in α is minimal and does not show a direct relationship with grouting. The normalized damping ratio curves also display an increase in reference strain with grouting. However, the damping ratio trends do not directly show this trend intuitively.

Grouted joints displayed the earliest increase in damping ratio with increased strain as well as the largest amount of increase. This implies that although grouting leads to the improvement of rock masses, they are more susceptible and dependent on the strain levels compared to jointed rocks. Another issue with the damping ratio is the methodology. The half power bandwidth method is comparatively less accurate in determining the damping ratio of soils or rocks compared to other methods such as the free vibration decay method. Further studies can be conducted on the comparison between different damping ratio calculation methodologies.

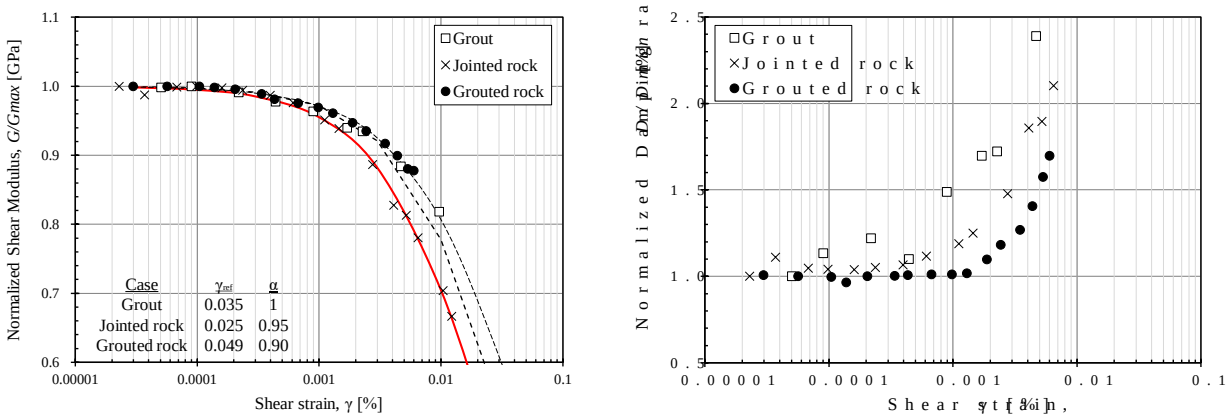

(a) Normalized shear modulus (b) Normalized damping ratio

Fig. 4 Normalized strain-dependent properties of grout, jointed rock and grouted rock specimens

4. CONCLUSION

In this study, the changes in nonlinear strain-dependent properties of jointed rocks with grouting were analyzed using resonant column tests conducted at 1000 kPa axial stress. The grouted rock specimen displayed increased shear modulus and decreased damping ratio for all tested strain levels compared to the jointed rock specimen. The maximum shear modulus increased by 262% and the minimum damping ratio decreased by 44.4% with grouting. The normalized modulus degradation curves of the grout, jointed rock and grouted rock specimens indicate that the shear

behavior of grouted rocks are governed by the strain-dependent properties of the grout material.

5. ACKNOWLEDGEMENT

This research was supported by the "Development of key subsea tunneling technology" program (16SCIPB066321-03) funded by the Korea Agency for Infrastructure Technology Advancement (KAIA) and the “U City Master and Doctor Course Grant (Education) Program” under the Korea Ministry of Land, Infrastructure and Transport (MOLIT).

REFERENCES

Acar, Y.B. and El-Tahir, E.T.A. (1986), "Low strain dynamic properties of artificially cemented sand", *J. Geotech. Eng.*, ASCE, **112**(11), 1001-1015.

Cha, M., Cho, G.C., and Santamarina, J.C. (2009), "Long-wavelength P-wave and S-wave propagation in jointed rock masses", *Geophysics*, **74**(5), E205-E214.

Chong, S.H., Kim, J.W., and Cho, G.C. (2014), "Rock Mass Dynamic Test Apparatus for Estimating the Strain-Dependent Dynamic Properties of Jointed Rock Masses", *Geotech. Test. J.*, **37**(2), 311-318.

Dano, C., Hicher, P.Y., and Tailliez, S. (2004), "Engineering properties of grouted sands", *J. Geotech. Geoenviron. Eng.*, **130**(3), 328-338.

Delfosse-Ribay, E., Djeran-Maigre, I., Cabrillac, R., and Gouvenot, D. (2004), "Shear modulus and damping ratio of grouted sand", *Soil. Dyn. Earthq. Eng.*, **24**(6), 461-471.

Fratta, D., and Santamarina, J.C. (2002), "Shear wave propagation in jointed rock: State of stress", *Géotechnique*, **52**(7), 495-505.

Gouvenot, D. (1987), "Injection des sols et législation relative aux nappes phréatiques", *Proc., Comptes-Rendus des Journées d’Études Internationales de l’AFTES*, 455-459.

Kim, J.W. (2008), “*Development of RMDT Apparatus to Characterize Strain-dependent Elastic Wave Propagation in a Jointed Rockmass*”, M.S. Thesis, Korea Advanced Institute of Science and Technology, Daejeon, Republic of Korea, 102.

Mollamahmutoglu, M., and Yilmaz, Y. (2011), "Engineering properties of medium-to-fine sands injected with microfine cement grout", *Mar. Georesour. Geotec.*, **29**(2), 95-109.

Pantazopoulos, I.A., and Atmatzidis, D.K. (2012), "Dynamic properties of microfine cement grouted sands", *Soil. Dyn. Earthq. Eng.,* **42**, 17-31.

Park, H.G., Sung, S.K., Park, C.G., and Won, J.P. (2008), "Influence of a C12A7 mineral-based accelerator on the strength and durability of shotcrete", *Cement. Concrete. Res*., **38**(3), 379-385.

Porcino, D., Marcianò, V., and Granata, R. (2012), "Static and dynamic properties of a lightly cemented silicate-grouted sand", *Can. Geotech. J.*, **49**(10), 1117-1133.

Richart, F. E., Hall, J. R., and Woods, R. D. (1970), "*Vibrations of soils and foundations*".

Tsai, P.H. and S.H. Ni (2012), "Effects of types of additives on dynamic properties of cement stabilized soils", *Int. J. Appl. Sci. Eng.*, **10**(2), 131-144.

Warner, J. (2004), *Practical handbook of grouting: soil, rock, and structures*, John Wiley & Sons. 720 pages.